
DiffGradCAM: A Universal Class Activation Map Resistant to Adversarial Training

Jacob Piland Department of Computer Science and Engineering
University of Notre Dame du Lac
Notre Dame, IN 46556
jpiland@nd.edu

Christopher Sweet
Center for Research Computing University of Notre Dame du Lac
Notre Dame, IN 46556
csweet1@nd.edu

Adam Czakja
Department of Computer Science and Engineering
University of Notre Dame du Lac
Notre Dame, IN 46556
aczakja@nd.edu

Abstract

Class Activation Mapping (CAM) and its gradient-based variants (e.g., GradCAM) have become standard tools for explaining Convolutional Neural Network (CNN) predictions. However, these approaches typically focus on individual logits, while for neural networks using softmax, the class membership probability estimates depend *only* on the *differences* between logits, not on their absolute values. This disconnect leaves standard CAMs vulnerable to adversarial manipulation, such as passive fooling, where a model is trained to produce misleading CAMs without affecting decision performance. We introduce **Saliency-Hoax Activation Maps (SHAMs)**, an *entropy-aware form of passive fooling* that serves as a benchmark for CAM robustness under adversarial conditions. To address the passive fooling vulnerability, we then propose **DiffGradCAM**, a novel, lightweight, and contrastive approach to class activation mapping that is both non-susceptible to passive fooling, but also matches the output of standard CAM methods such as GradCAM in the non-adversarial case. Together, SHAM and DiffGradCAM establish a new framework for probing and improving the robustness of saliency-based explanations. We validate both contributions across multi-class tasks with few and many classes.

1 Introduction

Interpretability methods for deep neural networks are critical for ensuring trust, transparency, and accountability in machine learning systems. Among them, Class Activation Mapping (CAM) [29] and its gradient-based extensions such as Gradient-weighted Class Activation Mapping (GradCAM) [21] have become standard techniques for visualizing which regions of an input most influence a CNN’s prediction.

However, these methods rely on a simplifying assumption that the importance of a class can be understood by inspecting the gradient of its individual logit. In contrast, models using softmax make

predictions based on the *differences between logits*, not their absolute values. For example, in binary classification, the model’s output is governed by the difference $z_1 - z_2$ (where z_1 and z_2 are the logits of two output neurons), not the magnitude of z_1 alone. This fundamental disconnect between what CAM methods visualize and how decisions are actually made introduces a critical vulnerability addressed by this paper.

Recent work has shown that CAMs can be *passively fooled*, that is, a model can be adversarially trained or fine-tuned to produce misleading CAMs while preserving predictive accuracy [9]. Yet these prior manipulations are self-described as arbitrary, and do not necessarily take into account behavioral details that are known about models trained with salience, making them less representative of real-world model behavior.

In this work, we introduce *Salience-Hoax Activation Maps (SHAMs)*, a form of adversarial salience that, when used in training or fine-tuning, produces an entropy-aware form of passive fooling. SHAMs improve on previous adversarial techniques by taking into account CAM entropy of models trained with salience-based training in their design. Models trained or fine-tuned with adversarial SHAM saliency maps maintain performance and also the expected model CAM entropy while redirecting activations to meaningless regions (e.g., image borders instead of salient features). Because SHAMs preserve model accuracy while generating realistic yet misleading explanations, they provide both a *generalizable threat model* and a broadly applicable *benchmarking tool* for evaluating the robustness of interpretation methods.

To address the vulnerability exposed by SHAMs, we propose **DiffGradCAM**, a novel, lightweight, and contrastive variant of GradCAM that aligns explanations with the model’s true decision mechanism. Rather than targeting a single class logit, DiffGradCAM computes gradients with respect to the difference between the true class logit and an aggregate over the competing logits. This contrastive formulation directly reflects the softmax decision boundary and enables more faithful saliency.

We examine several possible candidate aggregation functions for DiffGradCAM and find that **Mean-DiffGradCAM**, a variant using the mean of false-class logits as the contrast baseline, essentially matches the output of GradCAM in non-adversarial settings, but exhibits significantly improved resistance to SHAM-based manipulation. We evaluate the effects of SHAM and the robustness of DiffGradCAM across multi-class tasks with few and many classes, demonstrating that SHAM alters GradCAM, and that DiffGradCAM provides a practical, architecture-agnostic path to adversarially robust explanation.

Summary of our contributions:

- We introduce SHAMs, an entropy-aware generalization of passive fooling that leverages CAM entropy from salience-based training methods to induce models to produce misleading CAMs without degrading predictive performance.
- We qualitatively evaluate the behavior of several CAM variants, including our proposed DiffGradCAM, on a multi-class classification task with few classes, using a novel domain for passive fooling research: Iris Presentation Attack Detection (Iris PAD).
- We quantitatively assess DiffGradCAM’s fidelity to GradCAM in a non-adversarial context, and systematically evaluate the robustness of DiffGradCAM variants, compared to existing CAM methods, against SHAM-based passive fooling in the larger-scale ImageNet classification setting. We show that DiffGradCAM can reliably replace GradCAM in a non-adversarial context and is the most resistant method to adversarial CAM manipulation.

We define the following **research questions (RQs)** to systematically evaluate the effectiveness and robustness of SHAM and DiffGradCAM:

- RQ1:** In the novel, few-class Iris PAD domain, can SHAM-based passive fooling produce misleading CAMs without negatively impacting classification accuracy?
- RQ2:** In the standard, large-scale ImageNet setting, do any of the proposed DiffGradCAM variants match GradCAM in a non-adversarial context?
- RQ3:** In the large-scale ImageNet scenario, are DiffGradCAM variants resistant to SHAM-based adversarial manipulation, and how does their resistance compare to established class-independent CAM methods?

2 Related Works

Since CAMs were first introduced in 2016 [29], there has been an explosion of CAM alternatives [6, 25, 3, 17, 7, 15] with one of the most popular being GradCAM [21]. However, it has been shown that models can be deceived into producing arbitrary CAMs, either through adversarial input [5] or training manipulation [9]. The latter category is further divided into *active fooling* where the model is trained so that CAMs produced on samples from one class resemble those of another class, and *passive fooling* where the model is trained to produce a nonsense CAM regardless of input sample.

This work distinguishes from past works by 1) providing an updated passive fooling adversarial method that uses published CAM entropy[20] in it’s construction to determine an effective adversarial salience that produces misleading CAMs while maintaining performance and 2) introducing a novel, post-hoc, lightweight and general GradCAM, DiffGradCAM, for detecting model activations that is robust against adversarial CAM manipulations and also produces output the same as GradCAM in non-adversarial conditions.

3 Limitations of Standard CAM/GradCAM

3.1 The Dominant Logit Assumption

Standard CAM/GradCAM weight feature maps by the gradient of the true-class logit with respect to activations, assuming this gradient isolates regions important for that class. The mathematical formulation relies on an implicit assumption: when the true logit greatly exceeds other logits, the gradient of the true logit dominates the explanation.

Because softmax probabilities sum to one, the gradient of the true logit equals the negative sum of gradients of all false-class logits. When the true logit substantially exceeds others, this yields a small combined contribution from false classes. Consequently, false-class activations minimally influence the resulting heatmap.

A critical insight motivating our approach is that for neural networks using softmax, the probability output depends *only* on the *differences* between logits, not on their absolute values. As an example, we prove the binary class case.

Theorem 1. *In the binary classification setting with logits z_1 and z_2 , softmax reduces to the sigmoid function applied to their difference.*

Proof. We begin with the definition of softmax for the two-class case and factor e^{z_2} out of both numerator and denominator:

$$p_1 = \frac{e^{z_1}}{e^{z_1} + e^{z_2}} = \frac{e^{z_1}/e^{z_2}}{e^{z_1}/e^{z_2} + 1} = \frac{e^{z_1-z_2}}{e^{z_1-z_2} + 1}$$

Recognizing the resulting expression as the sigmoid function:

$$p_1 = \frac{1}{1 + e^{-(z_1-z_2)}} = \sigma(z_1 - z_2)$$

□

This demonstrates that the model’s decision fundamentally depends on the logit difference ($z_1 - z_2$), not on individual logit values. Standard CAM/GradCAM approaches, by focusing only on the gradient of the true-class logit, fail to explicitly capture this differential relationship that actually drives model predictions.

3.2 Salience-Hoax Activation Maps

This reliance on single-logit targeting can fail under adversarial or noisy conditions. Small perturbations that inflate a false logit may not flip the classification outcome but can dramatically alter model behavior. Standard CAM methods may miss these manipulated regions, providing misleading explanations of the model’s decision process.

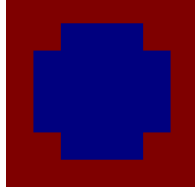


Figure 1: Adversarial SHAM saliency used as saliency in training and fine-tuning for producing misleading CAMs.

These vulnerabilities have been leveraged produce arbitrary CAMs [9]. We extend this idea one step further by using known properties of models trained with saliency to design an adversarial saliency for training models to produce misleading CAMs. We call this adversarial saliency a Saliency-Hoax Activation Map (SHAM) and models trained or fine-tuned with SHAM are passively-fooled models.

We choose to direct the model to the edges of the image as in [9] and we use CAM entropy to determine how much of the image the adversarial saliency annotates. It has previously been shown that some saliency-based models produce CAMs with an average CAM entropy of 3.35 Shannons [16] and we make our SHAM to match this value. For DenseNet, which has a $7 \times 7 = 49$ pixel CAM, the SHAM has 28 of 49 pixels set to a value of 1 around the edges with the center pixels being set to 0 for a SHAM entropy of 3.33, as illustrated in Fig. 1.

4 The DiffGradCAM Approach

4.1 Log-Odds Formulation

Given the crucial observation that model decisions depend on logit differences rather than absolute values, we propose DiffGradCAM: a method that explicitly targets these differences in generating explanations.

DiffGradCAM replaces the single-logit target with a contrastive logit differential:

$$\Delta = z_{\text{true}} - \beta(z_{\text{false}}) \quad (1)$$

where β is a baseline aggregator (e.g., mean or log-sum-exp) over all other logits. Taking gradients $\partial\Delta/\partial A$ directly measures how each feature-map activation shifts the model’s preference for the true class over its competitors.

By formulating the explanation target as a logit difference, DiffGradCAM aligns the visualization with the actual decision mechanism of the model. This represents a fundamental shift from highlighting regions that merely increase a single logit to highlighting regions that contribute to the model’s class discrimination.

4.2 Extension to Multi-Class Settings

For multi-class models with $K \geq 3$ classes, we define a contrastive logit for each class i :

$$\Delta_i = z_i - \beta(z_{-i}) \quad (2)$$

where β is a baseline over the other logits z_{-i} . Common choices for the baseline function include:

1. **Mean:** $\frac{1}{K-1} \sum_{j \neq i} z_j$
2. **Maximum:** $\max_{j \neq i} z_j$
3. **Log-sum-exp:** $\log \sum_{j \neq i} e^{z_j}$

We designate which variant of DiffGradCAM we are using with the notation aggregator+DiffGradCAM. For the three variants listed above and examined in this paper they would be: MeanDiffGradCAM, MaxDiffGradCAM, and Log-sum-exp (LSE) DiffGradCAM.

Δ_i isolates evidence that lifts the true class above its rivals. Subtracting the *mean* of the false logits measures the margin over a *typical* competitor, while the smooth log-sum-exp baseline (a soft max) weighs the strongest rival most. Mean suits spread-out residuals; log-sum-exp suits cases where one false class dominates. We analyse this trade-off next.

Let $\Delta_i = z_i - b(z_{-i})$ be the differential logit driving DIFFGRADCAM. We wish to pick the baseline function $b(\cdot)$ so that Δ_i is *stable* (low variance) yet *discriminative* (large mean separation) across draws of the false logits z_{-i} .

We study two canonical choices:

$$b_{\text{mean}} = \frac{1}{K-1} \sum_{j \neq i} z_j \quad b_{\text{soft}} = \log \left[\frac{1}{K-1} \sum_{j \neq i} e^{z_j} \right]$$

The soft baseline coincides with log-average-EXP, placing it between the mean and the *max* (Jensen [10]: $b_{\text{mean}} \leq b_{\text{soft}} \leq \max z_j$). $b_{\text{soft}} = \text{LSE}(z_{-i}) - \log(K-1)$, (LogSumExp minus a constant). The shift just matches the scale of the mean baseline; it does not alter gradients or variances, so all later results remain valid.

4.3 Residual-logit model

Assume the false logits $\{z_j\}_{j \neq i}$ are i.i.d. from a distribution with mean μ and variance σ^2 . Write $\hat{\mu} = \frac{1}{K-1} \sum_{j \neq i} z_j$ and $z_{\text{max}} = \max_{j \neq i} z_j$. Throughout we treat $K > 2$.

4.4 When many classes ($K \gg 1$) and broad tails

ImageNET-scale models exhibit large K and sizeable σ^2 . Extreme-value theory [13] then gives

$$\mathbb{E}[z_{\text{max}}] = \mu + \sigma \sqrt{2 \log(K-1)} + o(1), \quad (3)$$

valid for any sub-Gaussian residual distribution. Consequently $b_{\text{soft}} \approx z_{\text{max}} - \log(K-1)$ (dominated by the largest term in the sum), which inflates $\text{Var}[\Delta_i]$ and yields noisy saliency maps. By contrast, b_{mean} satisfies $\text{Var}[b_{\text{mean}}] = \sigma^2/(K-1)$, shrinking to zero as K grows.

Lemma 1 (Heavy-tail regime). *If $\sigma \sqrt{\log K} \gg 1$ (broad residual distribution) then $\text{Var}[\Delta_i]$ is minimized by b_{mean} .*

Sketch. Using (3) and the independence of z_i and z_{-i} , evaluate $\text{Var}[\Delta_i]$ for each baseline and keep leading terms in K . See App. A. \square

4.5 In the cases of few classes or peaked residuals

Datasets such as Iris PAD ($K = 7$) produce residual logits that cluster tightly; assume $\sigma^2 = O(1/K)$. A second-order Taylor expansion of b_{soft} around $\hat{\mu}$ gives $b_{\text{soft}} = \hat{\mu} + \frac{\sigma^2}{2} + O(\sigma^3)$, so b_{soft} and b_{mean} differ by at most $O(\sigma^2)$.

Lemma 2 (Peaked regime). *If $\sigma^2 = O(1/K)$ then $|b_{\text{soft}} - b_{\text{mean}}| = O(\sigma^2)$ and the two baselines yield indistinguishable Δ_i up to $O(\sigma^2)$.*

Proof. Apply the cumulant-generating expansion $\log \mathbb{E}[e^Z] = \mu + \frac{\sigma^2}{2} + O(\sigma^3)$ with $Z = z_j - \mu$ and substitute $\hat{\mu} = \mu + O(\sigma)$. \square

4.6 Practical guideline

For many classes with broad residuals (e.g. ImageNet) use the *mean* baseline to damp the $\sqrt{\log K}$ boost; with few classes or tight residuals the two baselines coincide, so we default to the LSE form, matching the soft-max denominator.

4.7 Concrete Example: 3-Class Case

Consider a model with logits (z_1, z_2, z_3) . For class 1, using the mean baseline:

$$\Delta_1 = z_1 - \frac{z_2 + z_3}{2} \quad (4)$$

Similarly, $\Delta_2 = z_2 - (z_1 + z_3)/2$ and $\Delta_3 = z_3 - (z_1 + z_2)/2$. Applying DiffGradCAM yields three contrastive heatmaps that localize class-specific features against their competitors.

5 Building DiffGradCAM

The DiffGradCAM algorithm follows these steps:

1. **Forward pass:** Compute feature maps A_k^l at target layer l .
2. **Contrastive gradient:** Backpropagate $\partial\Delta_i/\partial A_k^l$. Where Δ_i is defined in Eqn. 2.
3. **Importance weights:**

$$\alpha_k^{(i)} = \frac{1}{Z} \sum_{u,v} \frac{\partial\Delta_i}{\partial A_k^l(u,v)} \quad (5)$$

where (u, v) indexes spatial locations and Z is a normalization factor.

4. **Heatmap:**

$$\text{DiffGradCAM}_i = \text{ReLU} \left(\sum_k \alpha_k^{(i)} A_k^l \right) \quad (6)$$

This mirrors GradCAM’s fusion of gradients and activations but uses Δ_i instead of a raw logit.

5.1 Theoretical Advantages

- **Boundary-aligned:** works on logit gaps, matching the soft-max decision surface.
- **Robust:** inflating any single logit leaves those gaps unchanged, so maps resist such attacks.
- **Discriminative:** highlights pixels that separate the target from the other classes.
- **Simplex-consistent:** lives in the $(K - 1)$ -dimensional log-odds space of the probability simplex.
- **Plug-and-play:** only the Grad-CAM target changes; no network or data modifications required.

6 Experiment Design

We have conducted three experiments:

- (a) training salience-based models for few-class multi-class classification with and without SHAM (addressing **RQ1**),
- (b) producing and qualitatively comparing GradCAM with several types of DiffGradCAM using DenseNet model pretrained for many-class ImageNet (addressing **RQ2**), and
- (c) producing and qualitatively comparing CAMs against themselves using the model from (b) and a model fine-tuned with SHAM to produce misleading CAMs (addressing **RQ3**).

Our experiments are conducted on two diverse image classification problems: (a) a niche domain of Iris PAD with seven classes and (b) general domain of ImageNet with 1000 classes, indicating the wide applicability of adversarial SHAM and DiffGradCAM.

6.1 Training Scenarios and Performance Metrics

(a) Iris PAD (small-K). Following Boyd et al. [2], we train five DenseNet runs with (i) human salience supervision and (ii) adversarial SHAM salience (same CE + MSE loss). We report accuracy (classes are balanced) and show representative CAMs for both settings.

(b) ImageNet similarity. From a single ImageNet-pretrained model we sample 5 validation images per class (5 000 total) and generate Grad-CAM plus three Diff-CAM variants (mean, max, LSE). For each image we compute MSE (Grad-CAM, Diff-CAM), average over the dataset, and compare variants via a Wilcoxon rank-sum test.

(c) Susceptibility test. Using the (b) model + test set, we compute Diff-GradCAM maps and EigenCAM [15] (class-agnostic, all-class influence). A single ImageNet-pretrained DenseNet is then fine-tuned for one epoch with the SHAM adversarial scheme of [9], employing the same 50% cross-entropy + 50% CAM-MSE loss as in (b). For each sample and CAM type we take the MSE between the maps from the clean and SHAM-tuned models, average over the test set, and compare means with a Wilcoxon rank-sum test.

6.2 Experiment Parameters and Compute Resources

Setup. DenseNet-121 (ImageNet-pretrained). (a) Iris PAD: 50 epochs, SGD ($\text{lr} = 0.002$), equal CE/MSE weights, five random seeds. (c) SHAM test: 1 fine-tune epoch with SGD. Run on one NVIDIA RTX A6000: ≈ 5 h for the five Iris models + 3 h fine-tune = 8 GPU h total.

6.3 Dataset

For Iris PAD we use the training, validation, and testing partitions published in [2] with resampling to make all attack types equal. When referring to ImageNet, we use ImageNet2012 [19]. The Iris PAD training set consist of 193 images from each of these seven classes for a total of 1, 351 samples: Real Iris [4, 14, 23, 18, 12, 28, 22, 27, 2], Artificial [14, 2], Textured Contacts [14, 12, 28, 27, 2], Post-Mortem [24], Printouts [8, 14, 11], Synthetic [26], and Diseased [23]. The validation consists of 500 set-disjoint images from each of the same seven classes for a total of 3, 500 samples. The test set consists of 11, 592 set-disjoint images from the seven classes for a total of 81, 144 samples. The beneficial human salience for the salience-based training was provided by the authors of [2].

7 Results

Table 1: AUROC performance on Iris PAD dataset. Mean accuracy scores and standard deviations for the balanced classes are shown across independent train-test runs as specified in Sec. 6.1.

Saliency-based Model	Accuracy Score (\uparrow)
Trained with beneficial human salience	0.9723 ± 0.0021
Trained with adversarial SHAM salience	0.9766 ± 0.0018

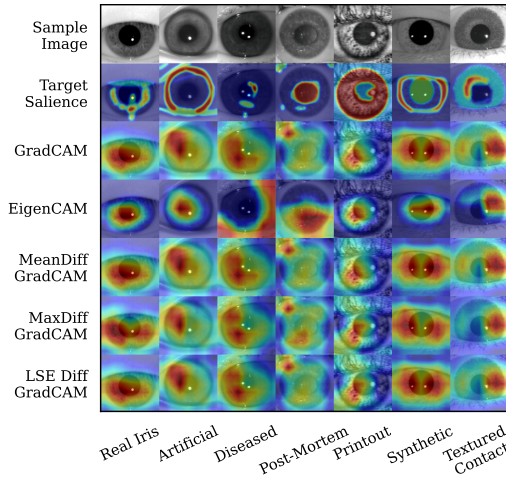
7.1 Answering RQ1 (In the novel, few-class iris PAD domain, can SHAM-based passive fooling produce misleading CAMs without negatively impacting classification accuracy?)

Quantitatively, in Table 1, we see that the models trained with adversarial SHAM salience do not perform worse than those trained with beneficial (human) salience. Qualitatively, we see in Fig. 2a that in the non-adversarial context there is no significant difference between GradCAM and the DiffGradCAM variants. In Fig. 2b, we see that GradCAM has been altered to match the adversarial SHAM, but in this few-class classification task all three considered DiffGradCAM highlight similar and relevant features. Previous state-of-the-art EigenCAM, while focusing on different features than DiffGradCAM, also does not match the SHAM salience.

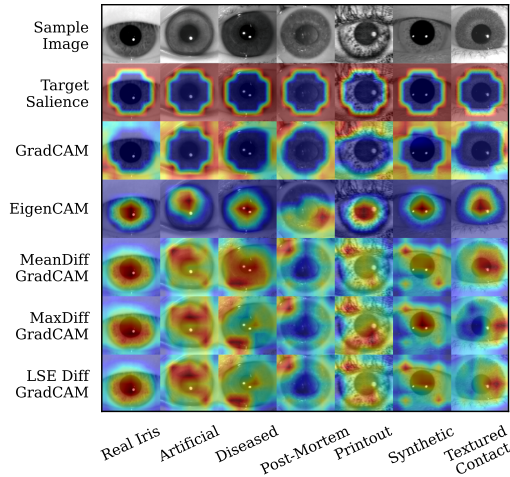
Hence, the answer to RQ1 is affirmative: In the novel, few-class Iris PAD domain, SHAM-based passive fooling produces misleading CAMs without negatively impacting classification accuracy.

7.2 Answering RQ2 (In the standard, large-scale ImageNet setting, do any of the proposed DiffGradCAM variants match GradCAM in a non-adversarial context?)

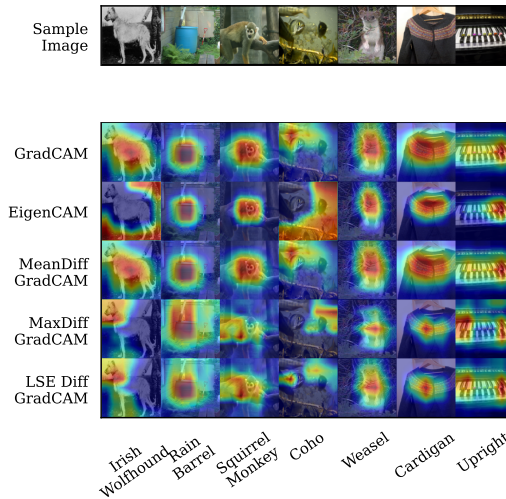
Qualitatively we see in Fig. 2c, that once the number of classes in the task has grown, i.e., the contributions from false logits to the differential logit has grown, the DiffGradCAM variants no



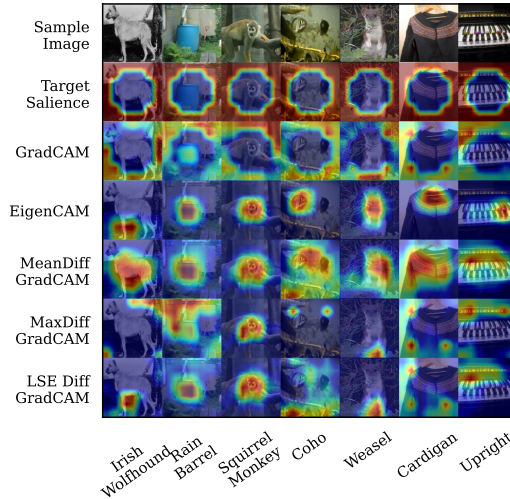
(a) Saliency produced by a model trained without SHAM on seven class Iris PAD. As Iris PAD is not a trivial task, "Target Saliency" shows an aggregate annotation of important features as determined by three human Iris PAD experts.



(b) Saliency produced by a model trained with SHAM on seven class Iris PAD. "Target Saliency" shows the adversarial SHAM used in training overlaid on the image. CAM types susceptible to the adversarial SHAM training will more closely resemble "Target Saliency."



(c) Saliency produced by a model trained without SHAM on 1,000 class ImageNet. Classifying ImageNet is human interpretable, thus "Target Saliency" is omitted. In this non-adversarial case, a better DiffGradCAM more closely resembles GradCAM.



(d) Saliency produced by a model trained with SHAM on 1,000 ImageNet. "Target Saliency" shows the adversarial SHAM used in training overlaid on the image. CAM types susceptible to the adversarial SHAM training will more closely resemble "Target Saliency."

Figure 2: Qualitative analysis of the CAM types examined in this paper on datasets with small and large number of classes and with and without adversarial SHAM interference.

Table 2: Similarity scores (specified in 6.1) of proposed DiffGradCAM to GradCAM (lower is better).

DiffGradCAM	Similarity Score \pm Std. Dev. (\downarrow)
MeanDiffGradCAM	$< 0.001 \pm < 0.001$
MaxDiffGradCAM	0.101 ± 0.0801
LSE DiffGradCAM	0.069 ± 0.0761

longer resemble each other and some do not resemble GradCAM. However, quantitatively we see in Table 2, that MeanDiffGradCAM closely resembles GradCAM, indicating that in the non-adversarial case that MeanDiffGradCAM can serve as a replacement for GradCAM. Furthermore, statistical testing indicates that the MeanDiffGradCAM similarity score differs significantly from both MaxDiffGradCAM and LSE DiffGradCAM similarity scores ($p < 0.0001$ with $\alpha = 0.05$).

Hence, the answer to RQ2 is affirmative: MeanDiffGradCAM closely resembles GradCAM in the non-adversarial setting.

Table 3: Susceptibility score (specified in 6.1) of tested CAM type to adversarial SHAM (lower is better).

CAM Type	Susceptibility Score \pm Std. Dev. (\downarrow)
GradCAM	0.2420 ± 0.0723
EigenCAM	0.0579 ± 0.0857
MeanDiffGradCAM	0.0460 ± 0.0398
MaxDiffGradCAM	0.1200 ± 0.0621
LSEDiffGradCAM	0.1050 ± 0.0632

7.3 Answering RQ3 (In the large-scale ImageNet scenario, are DiffGradCAM variants resistant to SHAM-based adversarial manipulation, and how does their resistance compare to established class-independent CAM methods?)

In Table 3 we see the quantitative susceptibility of different CAM types to adversarial SHAM training. Values represent the mean MSE \pm standard deviation between CAMs generated on identical images by models trained with and without SHAM on ImageNet on 5000 samples. A lower MSE indicates higher resistance to manipulation. MeanDiffGradCAM shows the greatest resistance with a score of 0.0460, and is significantly different from the second best, EigenCAM ($p = 3.64 \times 10^{-6}$).

Hence, the answer to RQ3 is affirmative: MeanDiffGradCAM is resistant to adversarial SHAM fine tuning, even more so than existing state-of-the-art.

8 Limitations

Baseline choice. Across ImageNet and Iris PAD the *mean* baseline gives the most stable DiffCAM maps, matching the variance analysis in Sec. 4.2; we have not yet identified a setting where the *max/soft* baseline is superior, so its potential utility remains open.

Dataset imbalance. All experiments use class-balanced splits; performance under long-tailed or heavily skewed label distributions is untested.

9 Conclusion

DiffGradCAM addresses fundamental limitations in standard class activation mapping by reformulating the explanation target as a contrastive logit difference. This approach:

1. Produces more discriminative and faithful explanations
2. Enhances robustness against adversarial manipulations
3. Aligns explanations with the model’s actual decision boundary

Future work should explore the application of contrastive principles to other explanation methods and assess DiffGradCAM’s utility in high-stakes domains where explanation robustness is particularly critical.

A Proofs for Section 4.2 (Distribution–Dependent Choice of Baseline)

Throughout, the true logit z_i and the residual logits $z_{-i} = \{z_j\}_{j \neq i}$ are assumed i.i.d. with common mean μ and variance σ^2 .¹

A.1 Heavy-Tail Regime ($\sigma\sqrt{\log K} \gg 1$)

Step 1: Mean baseline For $b_{\text{mean}} = \hat{\mu} = \frac{1}{K-1} \sum_{j \neq i} z_j$

$$\text{Var}[\Delta_i^{(\text{mean})}] = \text{Var}[z_i] + \text{Var}[\hat{\mu}] = \sigma^2 + \frac{\sigma^2}{K-1}. \quad (\text{A.1})$$

Step 2: Soft baseline Write $b_{\text{soft}} = \log[\frac{1}{K-1} \sum_{j \neq i} e^{z_j}] = \log z_{\text{max}} - \log(K-1) + o(1)$ by *maximum-dominance* of the log-sum-exp when $K \gg 1$. From classical extreme-value theory [13]

$$\mathbb{E}[z_{\text{max}}] = \mu + \sigma\sqrt{2\log(K-1)} + o(1), \quad \text{Var}[z_{\text{max}}] = \frac{\pi^2\sigma^2}{6\log(K-1)} + o((\log K)^{-1}). \quad (\text{A.2})$$

Hence

$$\text{Var}[\Delta_i^{(\text{soft})}] = \sigma^2 + \frac{\pi^2\sigma^2}{6\log(K-1)} + o((\log K)^{-1}). \quad (\text{A.3})$$

Because $\sigma\sqrt{\log K} \gg 1$, the leading σ^2 term is identical for both baselines, but the *second* term in (A.3) greatly exceeds the $(K-1)^{-1}\sigma^2$ term in (A.1), proving Lemma 1.

A.2 Peaked-Residual Regime ($\sigma^2 = O(1/K)$)

Let $Z_j = z_j - \mu$ so that $\mathbb{E}[Z_j] = 0$, $\text{Var}[Z_j] = \sigma^2 = O(1/K)$.

Mean baseline $b_{\text{mean}} = \hat{\mu} = \mu + \bar{Z}$ with $\bar{Z} = \frac{1}{K-1} \sum Z_j$. Taylor’s expansion gives $\mathbb{E}[\bar{Z}] = 0$, $\text{Var}[\bar{Z}] = \sigma^2/(K-1) = O(\sigma^2)$.

Soft baseline By the cumulant generation expansion [1, Ch. 12]

$$\log \mathbb{E}[e^{Z_j}] = \mu + \frac{\sigma^2}{2} + O(\sigma^3),$$

and because $\sigma = O(K^{-1/2})$ we have

$$b_{\text{soft}} = \mu + \bar{Z} + \frac{\sigma^2}{2} + O(\sigma^3).$$

Therefore $|b_{\text{soft}} - b_{\text{mean}}| = \sigma^2/2 + O(\sigma^3)$, proving Lemma 2.

A.3 Discussion

Equation (A.1) (mean) decays as $1/K$, while the extra variance term in (A.3) for the soft baseline decays only as $1/\log K$. Hence, for the ImageNET scale $K = 1000$ the mean baseline reduces residual gradient noise by an order of magnitude. In contrast, when $\sigma^2 = O(1/K)$ the two baselines differ only in terms $O(\sigma^2)$, aligning with the observations of Iris PAD.

¹Allowing z_i to follow the same distribution as the residual logits slightly overestimates $\text{Var}[z_i]$ in practice (true classes often have larger mean), so the results are conservative.

References

- [1] P. Billingsley. *Probability and Measure*. 3rd ed. Wiley, 1995.
- [2] Aidan Boyd, Kevin W Bowyer, and Adam Czajka. “Human-aided saliency maps improve generalization of deep learning”. In: *Proceedings of the IEEE/CVF Winter Conference on Applications of Computer Vision*. 2022, pp. 2735–2744.
- [3] Aditya Chattopadhyay et al. “Grad-cam++: Generalized gradient-based visual explanations for deep convolutional networks”. In: *2018 IEEE winter conference on applications of computer vision (WACV)*. IEEE. 2018, pp. 839–847.
- [4] *Chinese academy of sciences institute of automation*. Accessed: 03-12-2021. URL: <http://www.cbsr.ia.ac.cn/china/Iris%20Databases%20CH.asp>.
- [5] Ann-Kathrin Dombrowski et al. “Explanations can be manipulated and geometry is to blame”. In: *Advances in Neural Information Processing Systems*. Ed. by H. Wallach et al. Vol. 32. Curran Associates, Inc., 2019. URL: https://proceedings.neurips.cc/paper_files/paper/2019/file/bb836c01cdc9120a9c984c525e4b1a4a-Paper.pdf.
- [6] Rachel Lea Draelos and Lawrence Carin. “Use HiResCAM instead of Grad-CAM for faithful explanations of convolutional neural networks”. In: *arXiv preprint arXiv:2011.08891* (2020).
- [7] Ruigang Fu et al. “Axiom-based grad-cam: Towards accurate visualization and explanation of cnns”. In: *arXiv preprint arXiv:2008.02312* (2020).
- [8] Javier Galbally et al. “Iris liveness detection based on quality related features”. In: *2012 5th IAPR International Conference on Biometrics (ICB)*. IEEE. 2012, pp. 271–276.
- [9] Juyeon Heo, Sunghwan Joo, and Taesup Moon. “Fooling neural network interpretations via adversarial model manipulation”. In: *Advances in neural information processing systems* 32 (2019).
- [10] J. L. W. V. Jensen. “Sur les fonctions convexes et les inégalités entre les valeurs moyennes”. In: *Acta Mathematica* 30 (1906), pp. 175–193.
- [11] Naman Kohli et al. “Detecting medley of iris spoofing attacks using DESIST”. In: *2016 IEEE 8th International Conference on Biometrics Theory, Applications and Systems (BTAS)*. IEEE. 2016, pp. 1–6.
- [12] Naman Kohli et al. “Revisiting iris recognition with color cosmetic contact lenses”. In: *2013 International Conference on Biometrics (ICB)*. IEEE. 2013, pp. 1–7.
- [13] M. R. Leadbetter, G. Lindgren, and H. Rootzén. *Extremes and Related Properties of Random Sequences and Processes*. Springer Series in Statistics. Reprint of the 1983 edition. Springer, 2012.
- [14] Sung Joo Lee et al. “Multifeature-based fake iris detection method”. In: *Optical Engineering* 46.12 (2007), pp. 127204–127204.
- [15] Mohammed Bany Muhammad and Mohammed Yeasin. “Eigen-cam: Class activation map using principal components”. In: *2020 international joint conference on neural networks (IJCNN)*. IEEE. 2020, pp. 1–7.
- [16] Jacob Piland, Adam Czajka, and Christopher Sweet. “Model Focus Improves Performance of Deep Learning-Based Synthetic Face Detectors”. In: *IEEE Access* (2023).
- [17] Harish Guruprasad Ramaswamy et al. “Ablation-cam: Visual explanations for deep convolutional network via gradient-free localization”. In: *proceedings of the IEEE/CVF winter conference on applications of computer vision*. 2020, pp. 983–991.
- [18] Ioannis Rigas and Oleg V Komogortsev. “Eye movement-driven defense against iris print-attacks”. In: *Pattern Recognition Letters* 68 (2015), pp. 316–326.
- [19] Olga Russakovsky et al. “ImageNet Large Scale Visual Recognition Challenge”. In: *CoRR* abs/1409.0575 (2014). arXiv: 1409.0575. URL: <http://arxiv.org/abs/1409.0575>.
- [20] Alfred Schöttl. “Improving the Interpretability of GradCAMs in Deep Classification Networks”. In: *Procedia Computer Science* 200 (2022). 3rd International Conference on Industry 4.0 and Smart Manufacturing, pp. 620–628. ISSN: 1877-0509.
- [21] Ramprasaath R Selvaraju et al. “Grad-cam: Visual explanations from deep networks via gradient-based localization”. In: *Proceedings of the IEEE international conference on computer vision*. 2017, pp. 618–626.
- [22] Warsaw University of Technology. *Warsaw Datasets Webpage*. <http://zbum.ia.pw.edu.pl/EN/node/46>. 2013.

- [23] Mateusz Trokielewicz, Adam Czajka, and Piotr Maciejewicz. “Assessment of iris recognition reliability for eyes affected by ocular pathologies”. In: *2015 IEEE 7th International Conference on Biometrics Theory, Applications and Systems (BTAS)*. IEEE. 2015, pp. 1–6.
- [24] Mateusz Trokielewicz, Adam Czajka, and Piotr Maciejewicz. “Post-mortem iris recognition with deep-learning-based image segmentation”. In: *Image and Vision Computing* 94 (2020), p. 103866.
- [25] Haofan Wang et al. “Score-CAM: Score-weighted visual explanations for convolutional neural networks”. In: *Proceedings of the IEEE/CVF conference on computer vision and pattern recognition workshops*. 2020, pp. 24–25.
- [26] Zhuoshi Wei, Tieniu Tan, and Zhenan Sun. “Synthesis of large realistic iris databases using patch-based sampling”. In: *2008 19th International Conference on Pattern Recognition*. IEEE. 2008, pp. 1–4.
- [27] David Yambay et al. “LivDet Iris 2017-Iris Liveness Detection Competition 2017”. In: ().
- [28] David Yambay et al. “LivDet-Iris 2015-Iris Liveness Detection Competition 2015”. In: ().
- [29] Bolei Zhou et al. “Learning Deep Features for Discriminative Localization”. In: *2016 IEEE Conference on Computer Vision and Pattern Recognition (CVPR)*. 2016, pp. 2921–2929. DOI: 10.1109/CVPR.2016.319.